Catal Lett (2009) 130:185–191
DOI 10.1007/s10562-009-9849-6

Oxidation of Glycerol with Oxygen in a Base-free Aqueous Solution over Pt/AC and Pt/MWNTs Catalysts

Jing Gao · Dan Liang · Ping Chen · Zhaoyin Hou · Xiaoming Zheng

Received: 5 November 2008 / Accepted: 1 January 2009 / Published online: 17 January 2009

Abstract Catalytic oxidation of glycerol with molecular oxygen to glyceric acid was performed in a base-free aqueous solution over Pt/MWNTs and Pt/AC catalysts. Pt/MWNTs was more active for the easier accessibility of Pt on the external wall of MWNTs, and the initial TOF reached 10.63 mmol min^{-1}/mmol-Pt. The easier accessibility of glycerol to Pt particles on MWNTs was confirmed by Raman.

Keywords Glycerol oxidation · Glyceric acid · Pt · MWNTs

1 Introduction

The use of biorenewable feedstock is of crucial importance for a sustainable society because of the rapidly rising price of crude oil. Biodiesel is a renewable biofuel which is popularly recommended for its recycle usage of CO_2 and lower emission of particles, CO and HC in exhaust. During biodiesel production via transesterification of oils from plants such as rape, soya and palm, 100 kg of glycerol (also known as glycerin) is produced for every ton of biodiesel. A major surplus of glycerol has resulted from the increasing expansion of biodiesel production, and currently disposal of surplus glycerol is by incineration. Catalytic conversion of glycerol to value-added products has attracted much attention in the past few years [1–3].

Among the published works, an increasing number of studies were focused on chemoselective oxidation of glycerol to valuable oxygenated derivatives such as glyceric acid (GLYA), dihydroxyacetone (DIHA), hydroxypyruvic acid (HPYA) and tartronic acid (TARAC) [4–16]. And now, these oxygenated derivatives are either synthesized via costly and polluting stoichiometric oxidants (e.g. potassium permanganate, nitric acid or chromic acid) or produced via fermentation processes of low productivity [6, 17]. But the reported catalytic synthesis routes depend strongly on the reaction conditions (pH, temperature, substrate to metal ratio) and the nature of catalyst (metal, particle size and support).

Kimura et al. [4] firstly reported the catalytic oxidation of glycerol in 1993. They found that GLYA was the main product on Pt/C during glycerol oxidation, but the conversion of glycerol was quite low without the addition of alkali. Besson et al. [5] investigated the oxidation of glycerol in a wide ranged pH value (2–11) on a series of catalysts, and they found that the selectivity to GLYA can reach 70% on Pd/C (at pH 11), while the selectivity of GLYA decreased to 55% on Pt/C (at pH 7). Hutchings and co-workers [6–8] performed the oxidation of glycerol over a series of Au-based catalysts. They disclosed that Au particles sized in 15–30 nm (on carbon and graphite) exhibited a higher selectivity to GLYA at a moderate glycerol conversion, but big sized Au particles (>50 nm) were inactive even in a strong basic solution. On the other hand, Prati and co-workers [9, 10] revealed that even the well-dispersed Au nanoparticles on carbon with a mean diameter centered at 6 nm could not maintain its initial selectivity at full conversion. Davis and co-workers [11] further summarized that 5 nm sized Au particles on carbon was more active at pH 13.8 than the larger particles and bulk Au. Claus [12] and co-workers reported that Au/carbon catalyst was more active than Au on oxides (TiO_2, MgO and Al_2O_3).

J. Gao · D. Liang · P. Chen · Z. Hou (✉) · X. Zheng
Key Lab of Applied Chemistry of Zhejiang Province, Department of Chemistry, Zhejiang University, Xixi Campus, Hangzhou 310028, People's Republic China
e-mail: zyhou@zju.edu.cn

In published works, mainly Au-based catalysts were investigated in the oxidation of glycerol, but supported Au catalysts were totally inactive without the help of NaOH [7]. The role of base such as NaOH is contributed to abstract H^+ from the primary hydroxyl groups of glycerol and to start reaction [5, 7]. However, problems are that the presence of base allows only production of the salt of GLYA and excessive base would lead environmental pollution. It was also found that supported Pd and Pt catalysts can give some selectivity to GLYA, but the main reaction products are considered to be non-desired C_1 by-products, e.g. CO_2, HCHO and HCOOH [7].

Multi-wall nanotubes (MWNTs) have been widely studied as supports for metal nanoparticles in catalytic hydrogenation and oxidation reactions because of its excellent electronic properties, good physical and chemical stability, and large surface area [18–20].

In present work, we want to investigate the oxidation of glycerol with molecular oxygen at atmospheric pressure in aqueous solution without adding any base over active carbon (AC) and MWNTs supported Pt catalysts. We found that Pt/MWNTs was more active than Pt/AC with a comparable platinum particle size in the absence of base. And the Raman spectra of glycerol adsorbed on Pt/MWNTs were investigated and discussed.

2 Experimental

2.1 Materials

Active carbon was supplied from Tangshan Jianxin Active Carbon Co., Ltd. MWNTs prepared by a conventional CVD method was purchased from Shenzhen Nanotech Port Co., Ltd. Glycerol (>99.0%), $H_2PtCl_6 \cdot 6H_2O$ (>99%) and reducing agent KBH_4 (≥98.0%) were purchased from Shanghai Chemical Reagent Co. (China).

Glyceric acid (40% w/w in water), 1,3-dihydroxyacetone dimer (98%), glycolic acid (GLYCA) (98%), glyoxylic acid (50% w/w aq. soln), tartronic acid (98%) and glyceraldehyde (GLYHYDE) (95%) were purchased from Alfa Aesar, SIGMA or TCI.

2.2 Catalysts Preparation

Active carbon and MWNTs were firstly pretreated in 30 wt% H_2O_2 at 50 °C under stirring for 5 and 24 h, respectively. The solid was filtered out, washed thoroughly with distilled water and dried under vacuum at 60 °C for 10 h. And then, an aqueous solution of H_2PtCl_6 was added dropwise into a stirred suspension of 2.0 g pretreated support. The slurry was stirred for 30 min at room temperature, treated in ultrasonic for 2 h, and further reduced by an aqueous solution of KBH_4. Finally, the catalyst was filtered and washed with distilled deionized water to remove residual chlorine. The loading amount of Pt was controlled and confirmed by ICP as 5.0 wt% of the support.

2.3 Glycerol Oxidation

Glycerol oxidation was performed in a three-neck flask (100 mL) equipped with gas supply system, magnetic stirrer, condenser and thermocouple. Fifty milliliter aqueous solution of glycerol (0.1 g mL^{-1}) and 0.50 g catalyst were added into the reactor. Once temperature reached 60 °C, O_2 (99.9%) was introduced into the reactor at 150 mL min^{-1} via a mass flow controller. After reaction, catalyst was filtered off and the aqueous solution was analyzed using a high-performance liquid chromatograph (Agilent 1100) equipped with a refractive index (RI) detector and a Zorbax SAX column (Agilent). All products were confirmed with the standard mass spectrum in database and that of the standard products purchased from Alfa Aesar, SIGMA or TCI.

2.4 Characterizations

The textural structure of AC, MWNTs and supported Pt catalysts was detected by N_2 equilibrium adsorption at −196 °C with a Coulter Omnisorp 100 CX apparatus. All

Table 1 Texture of the supports and catalysts and particle size of Pt

	S_{BET} (m^2 g^{-1})	V_{micro} (cm^3 g^{-1})	V_{meso} (cm^3 g^{-1})	Particle size (nm)	
				XRD[a]	TEM[b]
AC	1,492	0.66	0.36	–	–
Pt/AC	1,250	0.56	0.31	6.5	9.5
MWNTs	143	0.00	0.30	–	–
Pt/MWNTs	133	0.00	0.28	6.3	6.7

[a] Calculated according to Scherrer–Warren equation

[b] Calculated according to $d_{TEM} = \frac{\sum n_i d_i^3}{\sum n_i d_i^2}$ (n_i is the number of particles having a characteristic diameter d_i)

samples were pretreated in vacuum at 200 °C for 2 h. The textural data were calculated from the adsorption isotherms.

X-ray diffraction patterns (XRD) were detected on RIGAKU D/MAX 2550/PC diffractometer using Cu $K\alpha$ radiation at 40 kV and 100 mA. Diffraction data were recorded using a continuous scanning at a rate of 0.02°/s, and a step of 0.02°.

The morphologies and dimensions of catalysts were observed by scanning electron microscopy (SEM, HITACHI S-4700) and transmission electronic microscopy (TEM, JEOL-2020F) using an accelerating voltage of 200 kV.

Raman spectra were performed with a 325 nm line of a He–Cd laser (LabRAM, HR-800) with a resolution of 2 cm^{-1} at room temperature. The incident laser power at the sample was 2 mW. Adsorption of glycerol was performed in a three-neck flask (100 mL). Fifty milliliter aqueous solution of glycerol (0.1 g mL^{-1}) and 0.5 g catalyst were added into the flask and stirred for 3.5 h at 60 °C, and then catalyst was filtered off and washed before Raman detection.

3 Results and Discussion

3.1 Characterizations

The texture structure of pretreated supports and catalysts are summarized in Table 1. The calculated surface area of pretreated active carbon is 1,492 m^2 g^{-1} and the volumes of micropore and mesopore are 0.66 and 0.36 cm^3 g^{-1}. After Pt loading, these data of Pt/AC decreased to 1,250 m^2 g^{-1}, 0.56 and 0.31 cm^3 g^{-1}, respectively. Mainly mesopore (with a volume of 0.30 cm^3 g^{-1}) was detected in the pretreated MWNTs, and the detected surface area is 143 m^2 g^{-1}, which can be contributed to the inner hollow cavities and aggregated pores formed by interaction of isolated MWNTs [21]. The deposition of Pt on MWNTs did not have a pronounced effect on the surface area and the pore size distribution. These results indicated that a proportion of pore channel of AC in Pt/AC catalyst might be blocked by Pt particles that caused decrease of surface area and pore volumes. But Pt particles were deposited mainly on the external wall of MWNTs which was further testified in the following SEM and TEM analysis.

SEM micrographs of Pt/AC and Pt/MWNTs are presented in Fig. 1. It can be found that big active carbon particles in different size and shape are full of different sized pores and no Pt particles were detected under lower magnification (100 times, Fig. 1a). A proportion of larger

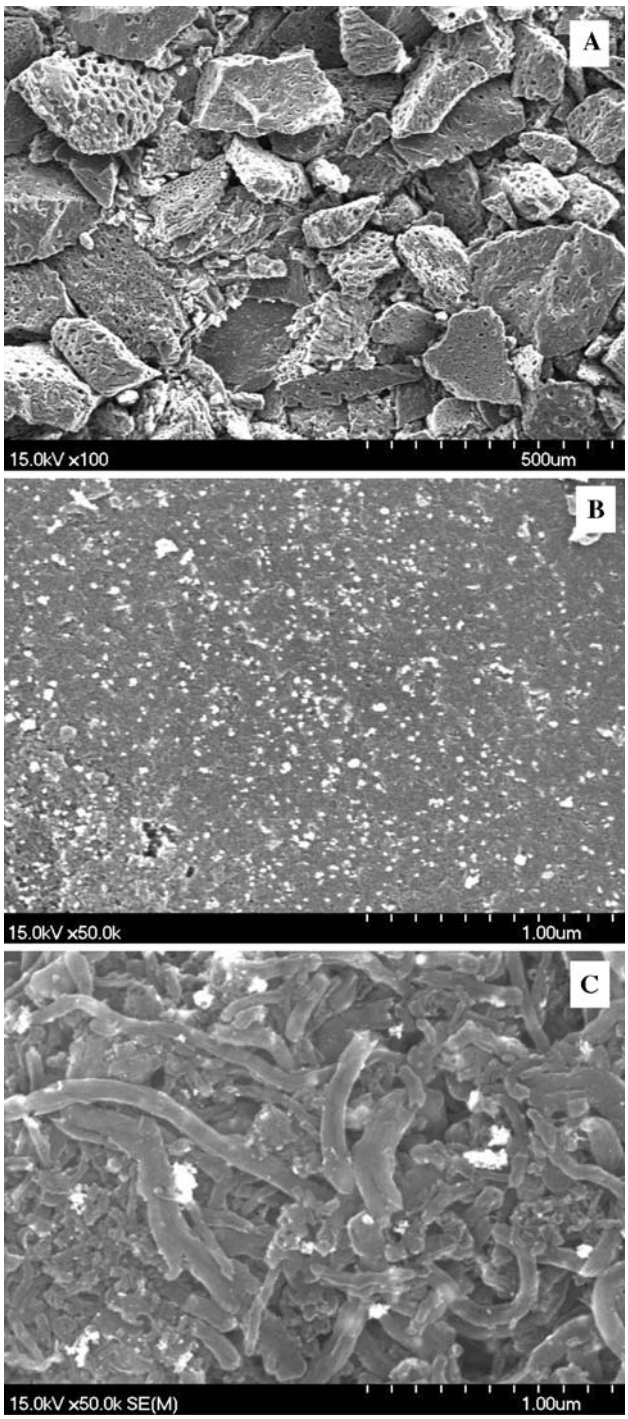

Fig. 1 SEM images of Pt/AC (**a**, **b**) and Pt/MWNTs (**c**)

platinum particles was detected on the external surface of both active carbon and MWNTs (50,000 magnifications, Fig. 1a, c). But the amount of bigger sized Pt particles on MWNTs is smaller than that on the surface of AC.

Figure 2 shows the typical TEM images of Pt/AC and Pt/MWNTs catalysts. The average particles size of Pt detected in TEM was calculated as:

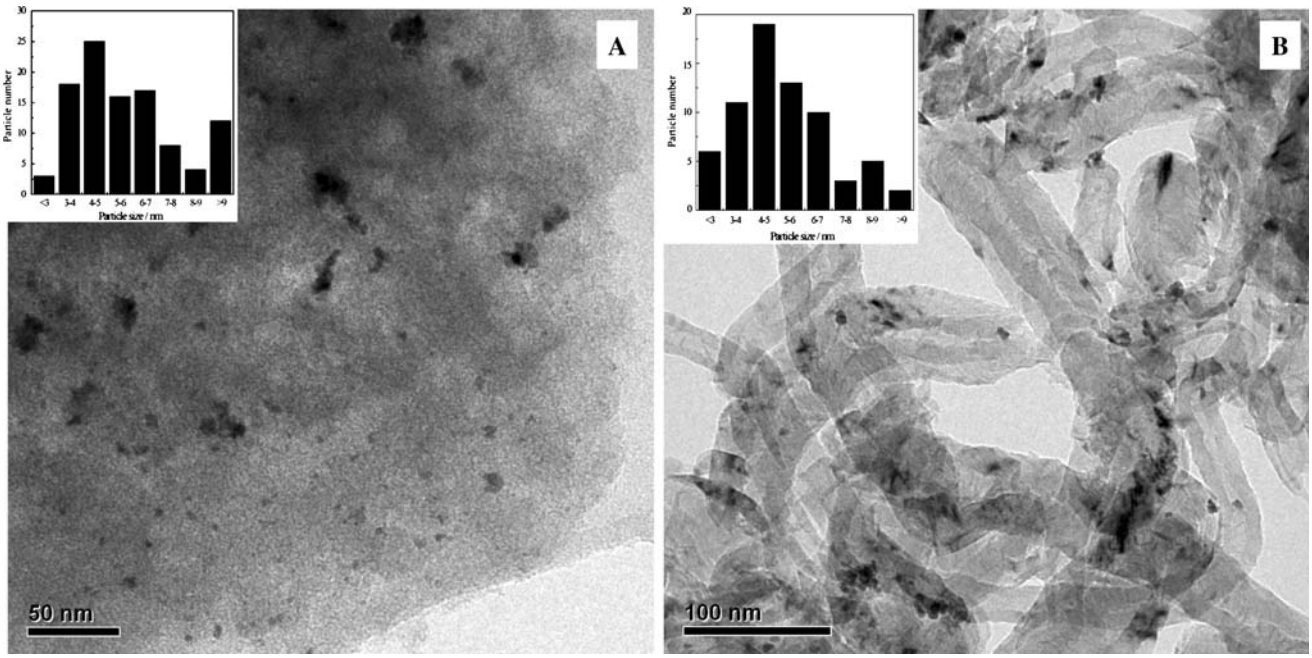

Fig. 2 TEM images of Pt/AC (**a**) and Pt/MWNTs (**b**)

$$d_{\mathrm{TEM}} = \frac{\sum n_i d_i^3}{\sum n_i d_i^2}$$

where n_i is the number of particles having a characteristic diameter d_i. The histograms of particle size distribution are inserted in the corresponding TEM images. It can be found that Pt particles dispersed unevenly on AC and the calculated mean Pt particle size was 9.5 nm (Fig. 2a). Figure 2b disclosed that the tips of MWNTs are sealed, and Pt particles distribute mainly on the outer wall of MWNTs. The dispersion of Pt on MWNTs is improved obviously compared with that on AC and the calculated Pt particle size is 6.7 nm.

Figure 3 shows the XRD spectra of Pt/AC and Pt/MWNTs catalysts. The typical diffraction peaks of cubic Pt crystallite were detected at 39.8°, 46.4° and 67.8° in both Pt/AC and Pt/MWNTs. According to Scherrer–Warren equation, the calculated crystalline sizes of Pt particle from the broadening of Pt (111) were 6.5 (in Pt/AC) and 6.3 nm (in Pt/MWNTs; see Table 1). Graphite was also detected in Pt/MWNTs. The crystalline size of Pt particle detected by XRD in Pt/AC is smaller than that detected by TEM, which might be contributed to that a proportion of Pt crystalline aggregated to bigger particles. And these aggregated Pt particles were clearly shown in Fig. 2a. But on the surface of Pt/MWNTs, this aggregation was depressed efficiently.

3.2 Glycerol Oxidation

Table 2 shows the catalytic activities of glycerol oxidation in a base-free aqueous solution at 60 °C for 6 h. Both AC and MWNTs were investigated under the same reaction condition, and no glycerol conversion was detected. On Pt/AC, the conversion of glycerol was 46.7% and the selectivity of GLYA was 59.5%. Surprisingly, the conversion of glycerol increased to 70.1% and the selectivity of GLYA reached to 69.8% over Pt/MWNTs. The calculated TOF on the basis of total Pt atoms was 0.58 and 0.87 min^{-1} on Pt/AC and Pt/MWNTs, respectively. And this TOF value (of Pt/MWNTs) in a base-free condition is

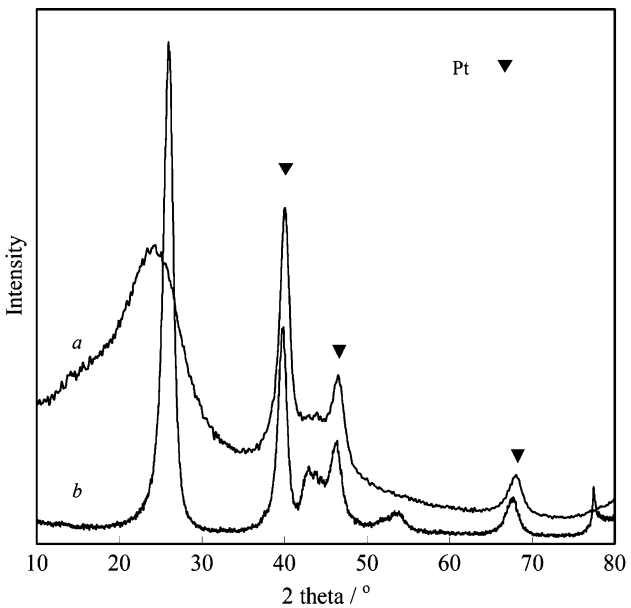

Fig. 3 XRD spectra of Pt/AC (*a*) and Pt/MWNTs (*b*)

Table 2 The activity and product distribution of glycerol oxidation on AC and MWNTs supported Pt catalysts

Samples	Conversion (%)	TOF[a] (min^{-1})	Selectivity (%)[b]					
			GLYA	DIHA	GLYCA	GLYHYDE	HPYA	C_1
AC	0.0	0.00	–	–	–	–	–	–
MWNTs	0.0	0.00	–	–	–	–	–	–
5Pt/AC	46.7	0.58	59.5	3.9	2.0	3.8	3.0	27.8
5Pt/MWNTs	70.1	0.87	69.8	2.8	2.2	3.0	0.0	22.2

Reaction conditions: 50 mL glycerol aqueous solution (0.1 g mL^{-1}), 0.5 g catalyst, glycerol/Pt molar ratio 445, $T = 60$ °C, $F_{o_2} = 150$ mL min^{-1}, 6 h

[a] *TOF* was calculated as: (mmol of converted glycerol)/(mmol of total Pt added)/(reaction time, min)

[b] Selectivity was calculated as: (mmol of product in reaction mixture)/(initial mmol of glycerol − mmol of glycerol left) × 100%

higher than that reported in reference [7] of Pt/C in the appearance of base at pH 11. Besides the desired GLYA, dihydroxyacetone (DIHA), glycolic acid (GLYCA), glyceraldehyde (GLYHYDE) and hydroxypyruvic acid (HPYA) were also detected in the liquid phase. During the reaction, trace amount non-desired C_1 by-products, e.g. CO_2 was detected in the air effluent; HCHO was detected in the liquid phase. And the total selectivities of these non-desired C_1 by-products were summarized in S_{C1}.

Table 3 summarized the time course of the glycerol oxidation on Pt/MWNTs. It can be found that the conversion of glycerol reached 25.2% with an 89.6% GLYA selectivity, and the calculated average TOF is 5.60 min^{-1} in the first 20 min. The selectivity of GLYA decreased to 70.9% in the first 2 h and then changed slightly in the followed 6 h. But the selectivity of C_1 increased with the increasing reaction time. Though the conversion of glycerol increased with the reaction time, the calculated TOF decreased. The dependence of the calculated TOF on the reaction time was shown in Fig. 4. From the plot in Fig. 4, it can be deduced that the initial TOF on Pt/MWNTs is 10.63 min^{-1}, which is higher than that reported in references [5, 7].

These results suggested that Pt/MWNTs catalyst was more active than Pt/AC for glycerol oxidation in absent of alkali. We suggest that Pt particles deposited on the external wall of MWNTs can contact easily with glycerol and/or oxygen, and the easier accessibility of Pt could contribute to a higher activity for glycerol oxidation in a base free condition. The lower activity of Pt/AC could be contributed to both the aggregation of Pt crystalline and the lower accessibility of same sized Pt in the pores of AC.

3.3 Raman Spectra of Adsorbed Glycerol

Figure 5 shows the Raman spectra of glycerol, fresh Pt/AC and Pt/MWNTs catalysts, and Pt/AC and Pt/MWNTs

Table 3 The time course of the glycerol oxidation on Pt/MWNTs

Time (min)	Conversion (%)	TOF[a] (min^{-1})	Selectivity (%)[b]					
			GLYA	DIHA	GLYCA	GLYHYDE	HPYA	C_1
20	25.2	5.60	89.6	2.0	0.0	0.0	0.0	8.4
40	32.4	3.60	77.5	4.8	3.5	0.0	0.0	14.2
60	37.1	2.75	76.4	3.7	1.9	2.9	0.0	15.1
80	41.8	2.33	75.5	4.3	3.3	3.7	0.0	13.2
100	45.2	2.01	73.1	3.4	2.7	3.8	0.0	17.0
120	48.1	1.78	70.9	4.6	3.3	4.2	0.0	17.0
180	57.1	1.41	72.7	3.1	1.6	4.3	0.0	18.3
240	61.1	1.13	73.1	3.6	3.2	4.4	0.0	15.7
300	67.9	1.01	73.3	3.1	3.2	3.7	0.0	16.7
360	70.1	0.87	69.7	2.8	2.1	3.0	0.0	22.4
420	74.8	0.79	69.7	3.0	2.6	2.6	0.0	22.1
480	79.7	0.74	70.5	2.6	3.7	3.1	0.0	20.1

Reaction conditions: 50 mL glycerol aqueous solution (0.1 g mL^{-1}), 0.5 g catalyst, glycerol/Pt molar ratio 445, $T = 60$ °C, $F_{o_2} = 150$ mL min^{-1}

[a] TOF was calculated as: (mmol of converted glycerol)/(mmol of total Pt added)/(reaction time, min)

[b] Selectivity was calculated as: (mmol of product in reaction mixture)/(initial mmol of glycerol − mmol of glycerol left) × 100%

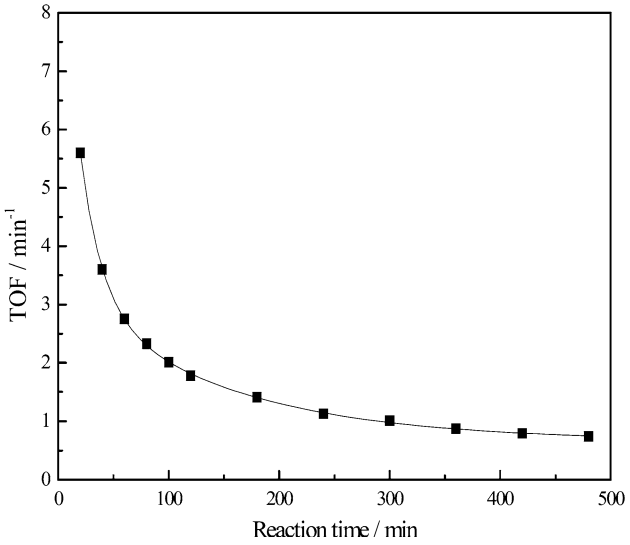

Fig. 4 The dependence of the calculated TOF on the reaction time

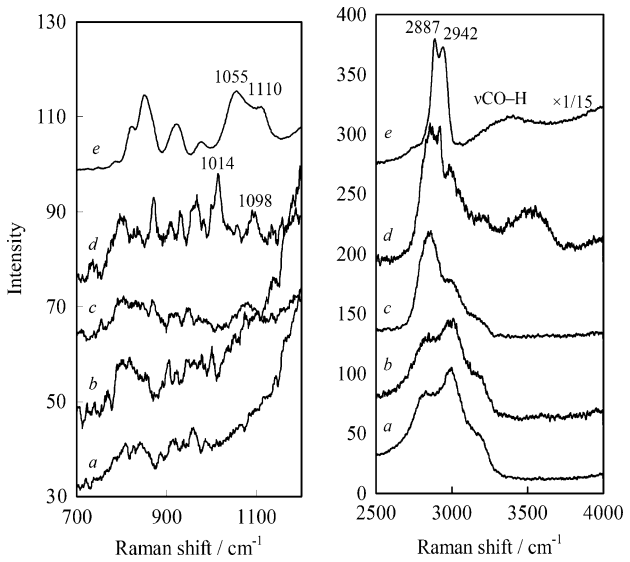

Fig. 5 Raman spectra of catalysts, glycerol adsorbed catalysts and neat glycerol *a* Pt/AC, *b* Pt/AC adsorbed glycerol, *c* Pt/MWNTs, *d* Pt/MWNTs adsorbed glycerol and *e* neat glycerol

catalysts after glycerol adsorption in 2,500–4,000 and 700–1,200 cm^{-1}. The intensity of neat glycerol was divided by 15. Raman peaks and assignments are summarized in Table 4. The broad Raman peaks of neat glycerol from 3,050 to 3,650 cm^{-1} region are assigned to the v_s(CO–H) and v_a(CO–H) of glycerol [22]. The bands at 2,887, 2,914 and 2,949 cm^{-1} are contributed to the $v_s(CH_2)$, $v_s(CH_2)_{FR}$ and $v_a(CH_2)$ of glycerol, respectively [23]. The peaks at 1,055 and 1,110 cm^{-1} come from the asymmetric stretch vibrations of the primary C–OH groups and of the secondary C–OH groups, respectively [24]. Peaks at 819 and 852 cm^{-1} are of the C–C stretching vibration and peaks at

Table 4 Raman peaks frequencies and assignments

Frequency (cm^{-1})		Assignment[a]
Neat glycerol	Glycerol adsorbed on Pt/MWNTs	
823, 853	–	v(C–C)
923, 977	–	CH_2 rock
1,055	1,014	v_s(C–OH) from the C-1, C-3
1,110	1,098	v_s(C–OH) from C-2
2,887	Overlapped	$v_s(CH_2)$
2,914	2,859	$v_s(CH_2)_{FR}$
2,949	2,923	$v_a(CH_2)$
3,050–3,650	3,337–3,760	v_s(CO–H), v_a(CO–H)

[a] Assignments taken from references [23, 24]

v Stretch, *a* asymmetric, *s* symmetric, *FR* Fermi resonance

923 and 977 cm^{-1} are assigned to rocking CH_2 vibrations in glycerol [23]. Similar Raman spectra of fresh Pt/AC catalyst and Pt/AC catalyst after glycerol adsorption were collected, which inferred that no adsorbed glycerol can be detected on Pt/AC. However, Raman peaks of adsorbed glycerol were detected on Pt/MWNTs after glycerol adsorption compared with the fresh Pt/MWNTs. These results indicated that glycerol adsorbed on Pt/MWNTs easily than that on Pt/AC.

Based on the above Raman analysis of neat glycerol, we speculate that the broad peak at 3,337–3,760 cm^{-1} in glycerol adsorbed on Pt/MWNTs is contributed to the v(CO–H) modes of adsorbed glycerol, which shifted to higher frequency than that of neat glycerol. The overlapped peaks at 2,859 and 2,923 cm^{-1} were tentatively assigned to the $v_s(CH_2)_{FR}$ and $v_a(CH_2)$ modes of adsorbed glycerol and the vibration of Pt/MWNTs. It is clearly that the $v_s(CH_2)_{FR}$ and $v_a(CH_2)$ of adsorbed glycerol shifted to lower frequency than neat glycerol. The peaks at 1,014 and 1,098 cm^{-1} were tentatively assigned to the v_s(C–OH) from the C-1 and from C-2, respectively, which also shifted to lower frequency. And the frequency of v_s(C–OH) from the C-1 decreased more obviously than v_s(C–OH) from the C-2. These results inferred that Pt particles on the external wall of MWNTs are easier accessible, this accessibility is of special importance for the reaction of glycerol as its viscosity is so higher (1,412 mPa s at 20 °C). And this advantage can explain the higher activity of Pt/MWNTs even in a base-free aqueous solution.

4 Conclusion

We found that Pt/MWNTs catalyst was more active than Pt/AC for glycerol oxidation with oxygen in a base free aqueous solution at 60 °C. N_2 adsorption, SEM and TEM

results disclosed that Pt particles mainly deposited on the external wall of MWNTs, which can contact easily with glycerol and/or oxygen. Raman spectra of adsorbed glycerol on Pt/MWNTs confirmed the easier accessibility of Pt particles.

Acknowledgment The Project Supported by Zhejiang Provincial Natural Science Foundation (Z406142), the National Natural Science Foundation of China (90610002) and the Ministry of Science and Technology of China through the National Key Project of Fundamental Research (2007CB210207).

References

1. Zhou CH, Beltramini JN, Fan YX, Lu GQ (2008) Chem Soc Rev 37:527
2. Centi G, van Santen RA (2007) Catalysis for renewables: from feedstock to energy production
3. Behr A, Eilting J, Irawadi K, Leschinski J, Lindner F (2008) Green Chem 10:13
4. Kimura H, Tsuto K, Wakisaka T, Kazumi Y, Inaya Y (1993) Appl Catal A Gen 96:217
5. Garcia R, Besson M, Gallezot P (1995) Appl Catal A Gen 127:165
6. Carrettin S, McMorn P, Johnston P, Griffin K, Hutchings GJ (2002) Chem Commun 696
7. Carrettin S, McMorn P, Johnston P, Griffin K, Kiely CJ, Hutchings GJ (2003) Phys Chem Chem Phys 5:1329
8. Carrettin S, McMorn P, Johnston P, Griffin K, Kiely CJ, Attard GA, Hutchings GJ (2004) Top Catal 27:131
9. Porta F, Prati L (2004) J Catal 224:397
10. Dimitratos N, Lopez-Sanchez JA, Lennon D, Porta F, Prati L, Villa A (2006) Catal Lett 108:147
11. Ketchie WC, Fang YL, Wong MS, Murayama M, Davis RJ (2007) J Catal 250:94
12. Demirel-Gulen S, Lucas M, Claus P (2005) Catal Today 102–103:166
13. Bianchi CL, Canton P, Dimitratos N, Porta F, Prati L (2005) Catal Today 102–103:203
14. Wang D, Villa A, Porta F, Su D, Prati L (2006) Chem Commun 1956
15. Ketchie WC, Murayama M, Davis RJ (2007) J Catal 250:264
16. Demirel S, Lehnert K, Lucas M, Claus P (2007) Appl Catal B Environ 70:637
17. Bauer R, Hekmat D (2006) Biotechnol Prog 22:278
18. Gu YJ, Wong WT (2006) Langmuir 22:11447
19. Guo GQ, Qin F, Yang D, Wang CC, Xu HL, Yang S (2008) Chem Mater 20:2291
20. Corma A, Garcia H, Leyva A (2005) J Mol Catal A Chem 230:97
21. Lemus-Yegres L, Such-Basanez I, Salinas-Martinez de Lecea C, Serp P, Roman-Martinez MC (2006) Carbon 44:587–610
22. Mudalige A, Pemberton JE (2007) Vib Spectrosc 45:27
23. Mendelovici E, Frost RL, Klooprogge T (2000) J Raman Spectrosc 31:1121
24. Kojima S (1993) J Mol Struct 294:193